Synthesis of Fe-ZrO_2 nanocomposite powders by reduction in H_2 of a nanocrystalline (Zr, Fe)O_2 solid solution

V.G. de Resende [a,*], F.L. Garcia [b], A. Peigney [b], E. De Grave [a], Ch. Laurent [b]

[a] *NUMAT, Department of Subatomic and Radiation Physics, University of Ghent, Proeftuinstraat 86, B-9000 Gent, Belgium*
[b] *CIRIMAT, UMR CNRS-UPS-INP, Université Paul-Sabatier, 31062 Toulouse cedex 9, France*

Keywords:
Nanocomposites
Nanoparticles
Iron-zirconia
Mössbauer spectroscopy

A B S T R A C T

The formation of Fe-ZrO_2 nanocomposite powders by reduction in hydrogen of a nanocrystalline totally stabilized $Zr_{0.9}Fe_{0.1}O_{1.95}$ solid solution was investigated by X-ray diffraction (XRD), field-emission-gun scanning electron microscopy (FEG-SEM) and Mössbauer spectroscopy. The reduction of the stabilized $Zr_{0.9}Fe_{0.1}O_{1.95}$ solid solution and the formation of metallic particles precedes the transformation of zirconia into the monoclinic phase, which becomes the major zirconia phase upon reduction at 950 °C. α-Fe particles with a size distribution slightly increasing from 10–50 to 20–70 nm upon the increase in reduction temperature are observed and a second population of smaller (<5 nm) γ-Fe nanoparticles is also noticed when the reduction is performed at 1000 °C. Another metallic phase with a hyperfine field of ~200 kOe at RT (~250 kOe at 80 K) is detected, which could account for an Fe/Zr phase. It could be formed by the reduction on an Fe^{2+}-rich transient phase incorporating a small fraction of the Zr^{4+} ions, formed by a phase partitioning process superimposed to the reduciton processes.

1. Introduction

Metal-oxide ceramic-matrix nanocomposite materials, where nanometric metal particles are dispersed in an oxide matrix, have attracted much interest owing to their exceptional optical, electrical, magnetic and mechanical properties [1–4]. Nanocomposite powders have been prepared directly by the mechanical mixing of powders [5,6] or by mechanosynthesis [7,8], or by chemical methods involving the reduction in hydrogen of suitable oxide precursors. There are several routes to prepare such oxide precursors. Intimate oxide mixtures have been obtained by the sol–gel route [9–14]. In earlier works, we have shown that oxide solid solutions prepared by decomposition and calcination of oxalate mixtures or by nitrate/urea combustion are also potentially high-performance precursors because the as-such produced materials feature a very homogeneous distribution of the desired metallic ions in their structures. Using the appropriate temperature and duration in the reduction process of these precursors, one is able to precisely control the micro/nanostructure of Fe/Cr-Al_2O_3 [15–19], Fe/Cr-Cr_2O_3 [20], Fe/Co/Ni-MgO [21,22] and Fe/Co/Ni-$MgAl_2O_4$ [23–25] nanocomposite powders. Although Ni-Y_2O_3-ZrO_2 composites are claimed to be materials of greater importance for solid-oxide fuel cells [26], Fe-ZrO_2 ceramic-matrix micro- or nanocomposites have been seldom studied. Fe-ZrO_2 microcomposites were prepared by melt infiltration [27] and mechanical mixing [28]. Axtell and Schalek [29] used mechanical milling to prepare Fe-ZrO_2 nanocomposite powders with interesting magnetic properties. Ringuede et al. [30] used a combustion/reduction method for the synthesis of Fe-Y_2O_3-ZrO_2 microcomposite powders with large Fe volume fractions (25 and 50%). The present paper presents results on the formation of Fe-ZrO_2 nanocomposite powders by reduction in hydrogen of a totally stabilized $Zr_{0.9}Fe_{0.1}O_{1.95}$ solid solution, the synthesis and characterization of which were reported elsewhere [31]. The study was performed using a combination of techniques including notably Mössbauer spectroscopy.

2. Experimental methods

The appropriate amounts of $Fe(NO_3)_3{\cdot}9H_2O$ and $ZrO(NO_3)_2{\cdot}xH_2O$ were dissolved in deionized water (20 mL, 70 °C) with seven times the so-called stoichiometric amount of urea, in order to produce 5 g of $Zr_{0.9}Fe_{0.1}O_{1.95}$ solid solution as described elsewhere [31]. The dish containing the solution was placed in a furnace pre-heated at 600 °C, keeping the door of the furnace open. After water evaporation, a smouldering combustion reaction takes place according to a redox reaction between the nitrates and urea, producing the oxide powder, which was characterized in detail [31]. Analysis of the XRD pattern only revealed the peaks of the tetragonal $Zr_{0.9}Fe_{0.1}O_{1.95}$ solid solution. Flash-combustion analysis revealed only trace amounts of carbon. The BET specific surface area was found equal to 39 m^2/g. FEG-SEM images revealed porous micro- or submicrometric grains, made up of smaller primary grains or crystallites about 10 nm in size, in good agreement to the size derived from the XRD pattern by the Scherrer method.

Batches of 0.08 g of the solid solution powder were reduced in H_2 atmosphere. The H_2 flow rate was equal to 15 L/h and the gas was dried on P_2O_5. The heating/cooling rate to the desired temperature (600, 700, 800, 900, 950 and 1000 °C)

* Corresponding author. Fax: +32 9 264 6697.
E-mail address: Valdirene.Gonzaga@Ugent.be (V.G. de Resende).

doi:10.1016/j.jallcom.2008.03.045

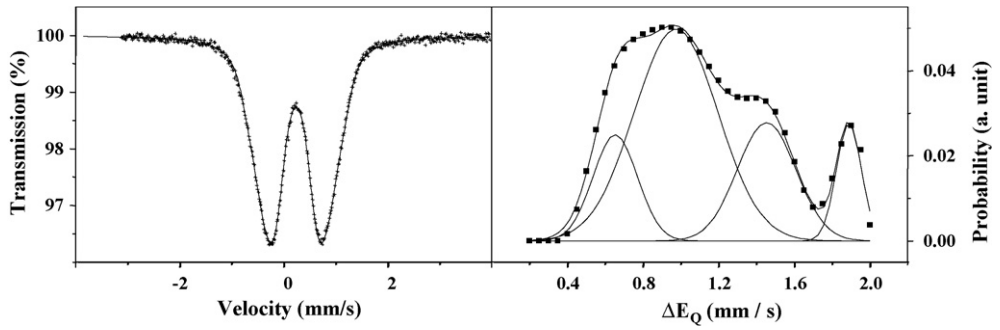

Fig. 1. Mössbauer spectra of the oxide solid solution at RT (left) and the corresponding QSD profiles (right).

and back to room temperature (RT) was 5 °C/min. No dwell was applied at the maximum temperature. Note that since the heating/cooling rate is small, one cannot consider that all runs are dependent upon the temperature only. On the contrary, a run at a given maximum temperature is an extension of an experiment performed at a lower temperature. The so-obtained powders will hereafter be denoted as R600, R700, . . . R1000.

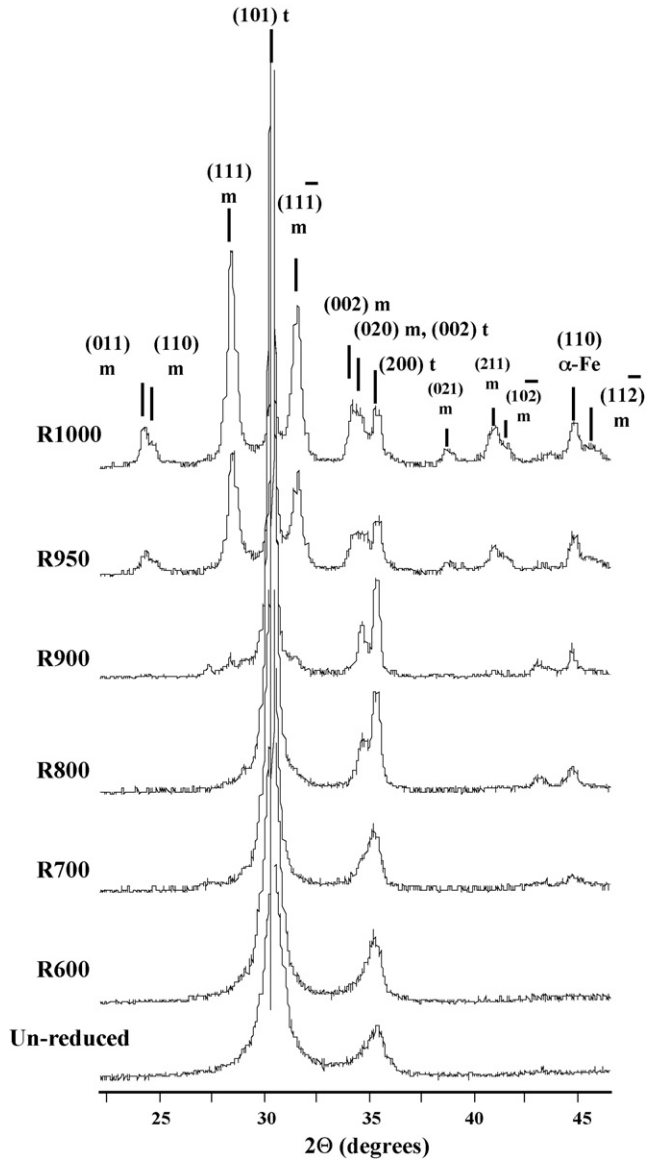

Fig. 2. XRD patterns of the oxide solid solution and of the Fe-ZrO_2 nanocomposite powders prepared by reduction in H_2 at different temperatures.

X-ray diffraction (XRD) patterns were recorded with a Brüker D4 Endeavor diffractometer using Cu Kα radiation. The proportions of tetragonal and monoclinic zirconia phases were evaluated from the XRD patterns using the Garvie–Nicholson method [32]. The powders were observed by field-emission-gun scanning electron microscopy (FEG-SEM JEOL JSM 6700F). ^{57}Fe Mössbauer spectra (MS) of the powders were collected with powders kept at 80 K and/or at room temperature, using a spectrometer operating in constant acceleration mode with triangular reference signal. ^{57}Co (Rh) source was used. Accumulation of data was performed in 1024 channels using a WISSEL CMCA-550 unit, and the measurements were run until a background of at least 10^6 counts per channel was reached. The spectrometer was regularly calibrated by collecting at RT the spectrum of a standard metallic iron foil or of a standard α-Fe_2O_3 powder. Isomer-shift values quoted hereafter are with respect to α-Fe at RT.

3. Results and discussion

The RT Mössbauer spectrum of the $Zr_{0.9}Fe_{0.1}O_{1.95}$ powder (Fig. 1) showed a broad quadrupole doublet, the shape of which could be adequately reproduced in terms of a model-independent quadrupole-splitting distribution (QSD). It was proposed [31] that although the solid solution is mainly tetragonal, as shown by analysis of the XRD pattern, it contains a significant fraction of the cubic phase. This suggestion indeed explained the multi-modal shape of the QSD profile evaluated from the RT doublet spectrum. This profile essentially consists of three contributions, i.e. two (characterized by maximum-probability quadrupole splittings of $\Delta E_{Q,m,1} = 0.65$ and $\Delta E_{Q,m,2} = 0.98$, respectively) supposedly arising from different environments of the Fe^{3+} cations in the tetragonal phase, and one ($\Delta E_{Q,m,3} = 1.45$) from the Fe^{3+} cations in the cubic phase. The minor fourth maximum in the QSD profile (ΔE_Q at ~1.9 mm/s) cannot be reasonably explained and was considered to be an artifact of the fitting.

The XRD patterns of the solid solution and the powders reduced in H_2 are shown in Fig. 2. The pattern for R600 is similar to that for the un-reduced solid solution. α-Fe is weakly detected for R700. Upon increasing the temperature to 1000 °C, the intensity of the (1 1 0) α-Fe peak gradually grows, inferring that the degree of reduction of the sample is progressing with the increase in temperature. For R800, a weak shoulder on the high-2θ side of the (1 0 1) t-ZrO_2 peak could indicate that a very low proportion of monoclinic zirconia is present. The latter phase is clearly detected for R900. The corresponding peaks become the dominant peaks in the XRD patterns for R950 (59%) and R1000 (85%). The steepest increase of the monoclinic XRD line intensities thus seems to take place for reduction temperatures between 900 and 950 °C. These observations could indicate that the begining of the selective reduction of the stabilized $Zr_{0.9}Fe_{0.1}O_{1.95}$ solid solution and the formation of α-Fe precedes the transformation of zirconia into the monoclinic phase.

FEG-SEM images of the reduced powders are presented in Fig. 3. For R600 (Fig. 3a–c), some round particles 10–50 nm in diameter (some of which are indicated by arrows on the images) are observed at the surface of large smooth ZrO_2 grains. These particles are to be

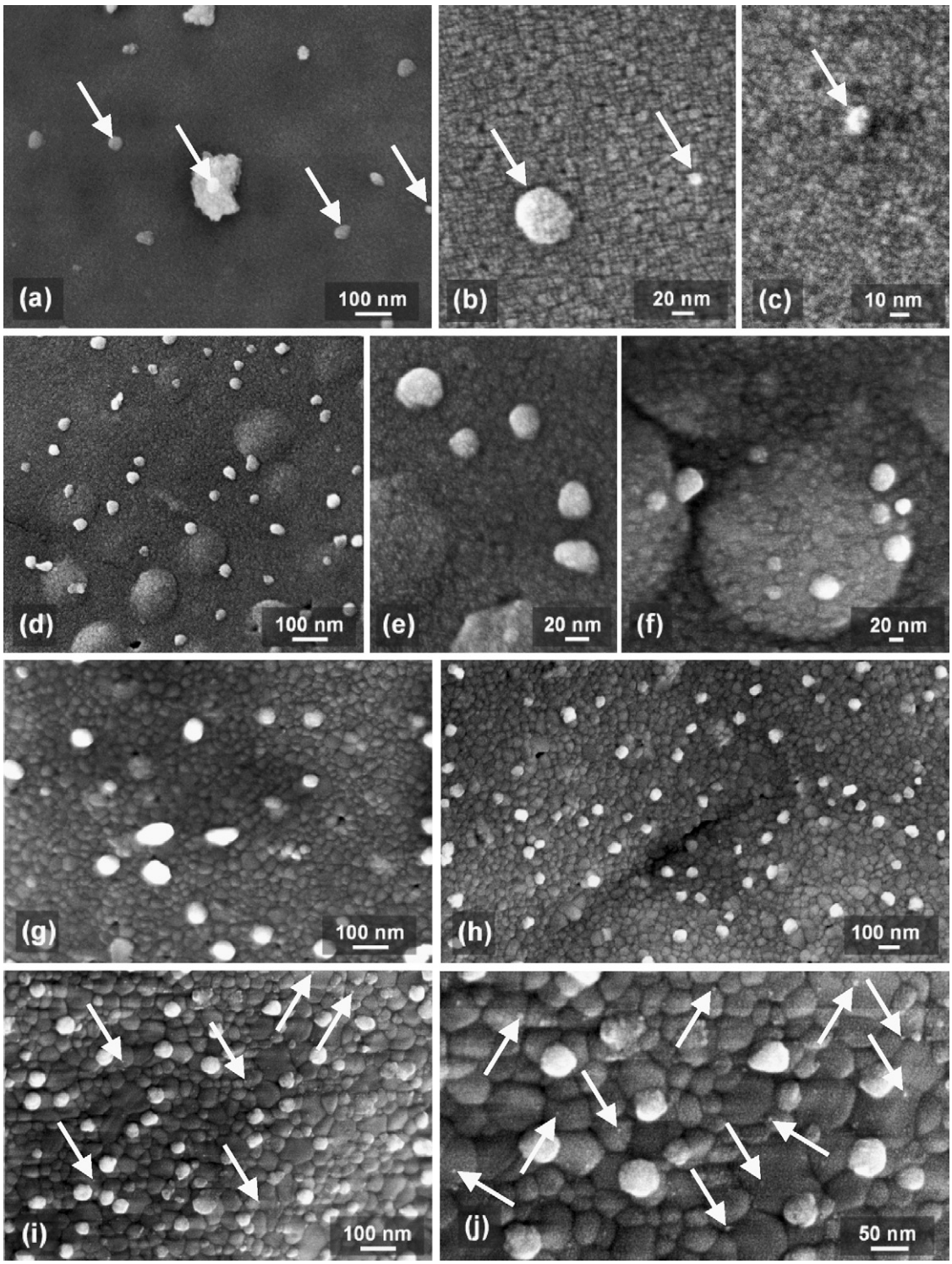

Fig. 3. FEG-SEM images of the Fe-ZrO_2 nanocomposite powders prepared by reduction in H_2 at 600 °C (a–c); 700 °C (d and e); 800 °C (f); 900 °C (g); 950 °C (h); 1000 °C (i and j).

distinguished from the few small zirconia grains appearing slightly larger and with irregular shapes (Fig. 3a). Note that in the center of Fig. 3a, a round α-Fe particle appears located on top of a zirconia grain. Higher magnification images (Fig. 3b and c) show Fe nanoparticles with diameters of 30, 15 and 12 nm (indicated by arrows on the images) on a granular surface which appear to be made up of clusters a few nanometers across due to the Pt metallization. Nevertheless, is possible to distinguish the boundaries of the zirconia crystallites (Fig. 3b) showing that their size is in the range 10–30 nm, remaining almost constant for R600, R700 (Fig. 3e) and R 800 (Fig. 3f). For R700 (Fig. 3d and e) and R 800 (Fig. 3f), the size distribution of the round Fe particles is roughly similar to that observed for R600, a few particles only being slightly larger (up to 60 nm). In Fig. 3f, one can observe some α-Fe particles clearly emerging from a circular-shaped grain in the oxide. Such circular forms are already observed at the surface of the grains of the oxide solid solution and do not appear from the evolution of the matrix during the selective reduction. For the R900 and R950 pow-

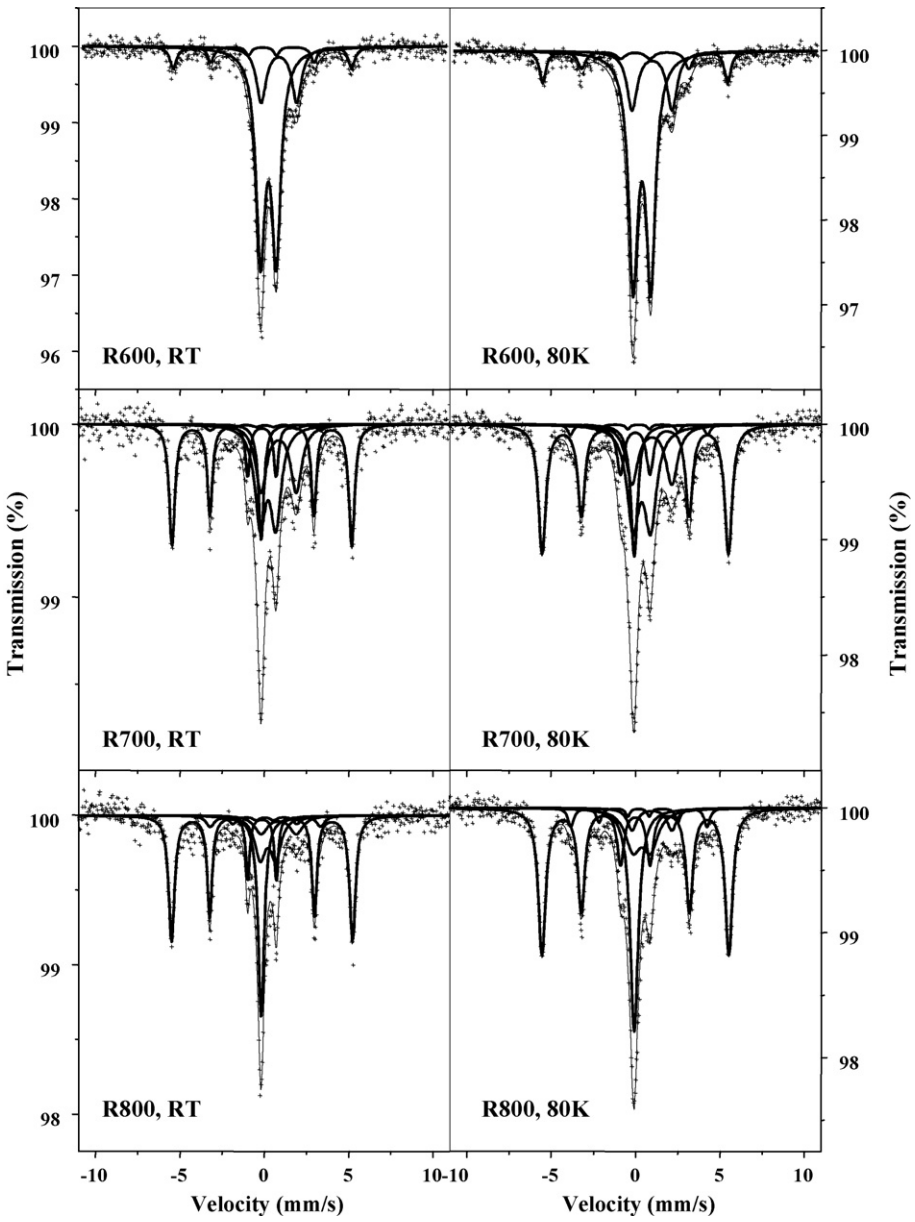

Fig. 4. Mössbauer spectra (RT and 80K) of the Fe-ZrO_2 nanocomposite powders prepared by reduction in H_2 at 600, 700 and 800 °C.

ders (Fig. 3g and h), the size distribution of the α-Fe particles is again slightly shifted to higher values (20–70 nm) and the matrix crystallites have grown significantly (maximal size 80 nm), reflecting the beginning of the formation of m-ZrO_2. The main novelty appear for the R1000 powder (Fig. 3i and j) in which many Fe particles smaller than 5 nm (some of which are indicated by arrows on the images) are clearly evidenced at the surface of most zirconia crystallites. For this powder, the larger Fe particles are still in the 20–70 nm size range but the matrix crystallite have grown and are in the range 30–120 nm (Fig. 3i and j), reflecting that m-ZrO_2 is now the major zirconia phase. Note that it is not possible to compare the relative quantities of large and small Fe particles in the different powders from such images since their population, in a particular powder, varies significantly from one observed area to another.

The MS at RT and at 80 K of the reduced powders (Figs. 4 and 5) were interpreted assuming discrete, symmetrical components with Lorentzian line shapes. The as-such adjusted values of some relevant Mössbauer parameters for the various subspectra resolved from these MS are listed in Table 1. The evolution of the relative areas RA of these subspectra as calculated from the 80 K data is shown in Fig. 6. Three components were found to be required to obtain an adequate fit for the MS of powder R600: (i) a sextet with hyperfine parameters typical of the α-Fe phase (which was not detected in the XRD pattern); (ii) a doublet that can be attributed to Fe^{3+} ions in the stabilized zirconia phase; (iii) a doublet that could account for Fe^{2+} ions in the stabilized zirconia phase, thus formed by reduction of part of the initial Fe^{3+} ions. Interestingly, the Fe^{2+} doublet parameters are close to those reported by Ghigna et al. [33] for interstitial Fe^{2+} ions in the cubic zirconia lattice. Moreover, the simultaneous presence of Fe^{3+}, Fe^{2+} and metallic Fe is in agreement with results reported by other researchers [34,35] showing that the reduction of a cubic $Zr_{0.8}Fe_{0.2}O_{1.8}$ solid solution in Ar–H_2 atmosphere proceeds in two steps: Fe^{3+} to Fe^{2+} and Fe^{2+} to metallic Fe. However, the reduction state of the iron species is still fairly low when the reduction is performed at only 600 °C (see RA values in Table 1). For R700, the proportion of α-Fe strongly increases at the expense of that of Fe^{3+} contribution and interestingly two more components are found: a central singlet that can be ascribed

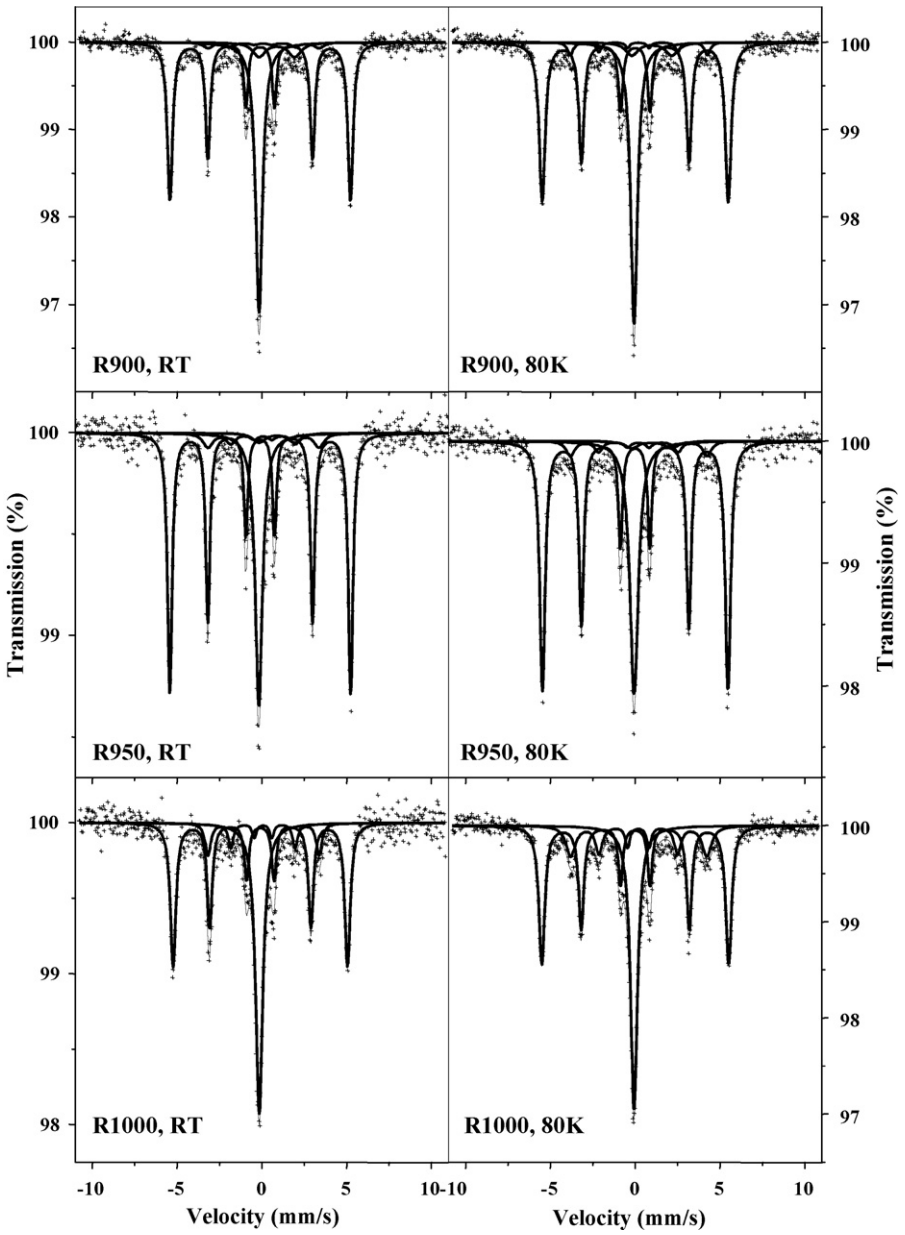

Fig. 5. Mössbauer spectra (RT and 80 K) of the Fe-ZrO_2 nanocomposite powders prepared by reduction in H_2 at 900, 950 and 1000 °C.

to the face-centered cubic γ-Fe phase and a very weak inner sextet with hyperfine field ~200 kOe at RT (~250 kOe at 80 K). As the reduction temperature is further raised, the reduction of the iron species progresses, which is reflected in the absence of the Fe^{3+} doublet above 800 °C and of the Fe^{2+} doublet for R1000 (Fig. 6a). The proportion of the α-Fe component increases from R700 to R950, but ends up lower for R1000, whereas the contribution of the γ-Fe component increases from R700 to R900 from where on it reaches a plateau (Fig. 6b). The RA value for the inner sextet is constant for R700-R950, but markedly increases for R1000, at the expense of α-Fe. The nature of the phase that gives rise to this inner sextet is puzzling. The hyperfine parameters of the sextet suggest an Fe/Zr phase, more specific identification remains impossible because of a lack of sufficiently reliable Mössbauer data for reference compositions.

The FEG-SEM studies revealed that some large (up to 50 nm) Fe particles are formed at the zirconia matrix surface upon reduction at a temperature as low as 600 °C. The size range of these particles could point to α-Fe, which would be in agreement with the MS data. It can reasonably be inferred that the quantity of such particles increases upon increasing the reduction temperature between 600 and 950 °C, because the MS study has shown an increasing proportion of α-Fe. However, the size distribution (20–70 nm) is only slightly larger for R950 than for R600. Thus, it could be possible to rule out a coalescence process which would lead to a more marked shift to larger sizes an to a wider size range. It is thus proposed that the α-Fe surface particles grow by diffusion of Fe probably from rather deep levels within the oxide matrix and along the crystallite boundaries, and also by surface diffusion at the zirconia grains surface. This process results in rather large α-Fe surface particles in moderate quantities. By contrast, much smaller (<5 nm) surface particles, in rather large quantities, are formed at higher temperature (1000 °C, maybe also at lower temperatures, notably 900 and 950 °C but with too small a size to be detected by FEG-SEM) and seem to correspond to the metallic Fe produced by each zirconia crystallite located at the surface. They could be attributed to γ-Fe

Table 1
Mössbauer results at RT and 80 K for the oxide solid solution reduced in H_2 at selected temperatures

T_R (°C)	α-Fe			Sextet			Fe^{3+} doublet[a]			Fe^{2+} doublet			γ-Fe	
	H_{hf}	RA	δ	H_{hf}	RA	δ	ΔE_Q	RA	δ	ΔE_Q	RA	δ	δ	RA
RT														
600[b]	327	11	0.00	–	–	–	0.93[c]	69	0.35[c]	2.10	20	0.98	–	–
700	330	39	−0.01	203[c]	3	0.18[c]	0.93[c]	28	0.35[c]	2.09[c]	21	0.98[c]	−0.06[c]	9
800	332	50	0.00	203[c]	6	0.18[c]	0.93[c]	15	0.35[c]	2.09[c]	8	0.98[c]	−0.06[c]	21
900	330	57	−0.01	203[c]	4	0.18[c]	–	–	–	2.09[c]	7	0.98[c]	−0.07	32
950	331	64	0.00	203[c]	7	0.18[c]	–	–	–	2.09[c]	3	0.98[c]	−0.08	26
1000[b]	329	53	0.00	203	12	0.18	–	–	–	–	–	–	−0.06	35
80 K														
600[b]	340	13	0.12	–	–	–	1.04	68	0.49	2.36	19	1.09	–	–
700	342	44	0.11	252	3	0.31[c]	1.04[c]	27	0.49[c]	2.36[c]	16	1.09[c]	0.04[c]	10
800	343	53	0.11	250	5	0.31[c]	1.04[c]	15	0.49[c]	2.36[c]	5	1.09[c]	0.04[c]	22
900	340	60	0.11	250	5	0.31[c]	–	–	–	2.36[c]	5	1.09[c]	0.04	30
950	339	66	0.11	250[c]	6	0.31[c]	–	–	–	2.36[c]	2	1.09[c]	0.04	26
1000[b]	341	51	0.11	249	18	0.31	–	–	–	–	–	–	0.04	31

The quadrupole splittings (ΔE_Q) and isomer shifts (δ) are given in mm/s, the hyperfine fields in kOe and the relative spectral areas (RA) are in % of total area. The values of isomer shifts are with respect to metallic iron.

[a] Hyperfine parameters for this doublet were fixed at the values obtained for the precursor material before reduction in H_2.

[b] Mössbauer parameters for these spectra were adjusted and their values were subsequently fixed in the numerical analyses of the spectra for samples reduced at other temperatures.

[c] Fixed parameter.

and/or the hypothetic Fe/Zr phase. During this stage, the diffusion process in the zirconia crystallites would be lattice diffusion.

Earlier studies by the present authors on the selective reduction in H_2 of Fe_2O_3–Cr_2O_3–Al_2O_3 [17], CoO–FeO–NiO–MgO [22] and $CoAl_2O_4$–$FeAl_2O_4$–$MgAl_2O_4$ [24,25] solid solutions have revealed that the reduction of the more easily reducible transition metal cation promotes the reduction of the less reducible one(s), resulting in the formation of Fe/Cr, Co/Fe/Ni and Co/Fe alloy nanoparticles, respectively. However, this promoting effect is not thought to be probable if the two M/M_xO_y systems are too far apart in the Ellingham diagram that plots the variation of the free energy ΔG of the oxidation reaction versus temperature, as is the case for Fe/Fe_2O_3 and Zr/ZrO_2, where ZrO_2 is considered to be unreducible. However, as mentioned above the Fe^{2+} doublet parameters are close to those reported by Ghigna et al. [33] for interstitial ions in the cubic zirconia lattice. Interestingly, these authors [33] have proposed that there is a direct iron-zirconium metallic bond since for the interstitial Fe^{2+} ions the shorter iron-zirconium distance is only 0.364 nm. Furthermore, it was shown [31] that when the stabilized $Zr_{0.9}Fe_{0.1}O_{1.95}$ solid solution is heated in air, the solubility of the Fe^{3+} progressively decreases which results in a phase partitioning with the formation of Zr^{4+}-substituted hematite nanoparticles at the surface of the zirconia grains. This indicates that it is indeed possible for the Zr^{4+} ions to leave their positions in the zirconia lattice to enter an iron-rich phase. Thus, we propose that as the reduction temperature is progressively increased and the reduction proceeds, there is the superimposition of the thermal effect, i.e. phase partitioning, resulting in the formation of an Fe^{2+}-rich transient phase incorporating a small fraction of the Zr^{4+} ions, which is easily reduced into a metallic Fe/Zr phase accounting for the particular sextet detected by MS.

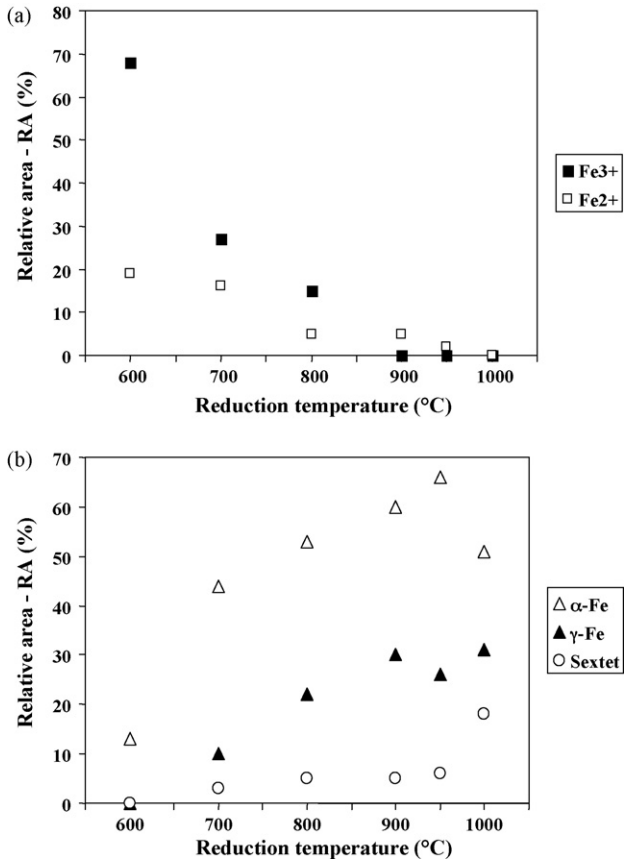

Fig. 6. Proportions of the unreduced iron species (a) and reduced iron species (b) in the Fe-ZrO_2 nanocomposite powders as calculated from the MS measured at 80 K versus the reduction temperature.

4. Conclusions

The formation of Fe-ZrO_2 nanocomposite powders by reduction in hydrogen of a totally stabilized $Zr_{0.9}Fe_{0.1}O_{1.95}$ solid solution (crystallite size below about 10 nm) was investigated by XRD, FEG-SEM and Mössbauer spectroscopy. The beginning of the reduction of the stabilized $Zr_{0.9}Fe_{0.1}O_{1.95}$ solid solution and the formation of metallic particles precedes the transformation of zirconia into the monoclinic phase, which becomes the major zirconia phase upon reduction at 950 °C (crystallite size 30–120 nm). α-Fe particles with a size distribution slightly increasing from 10–50 to 20–70 nm upon the increase in reduction temperature are observed and a second population of smaller (<5 nm) nanoparticles, probably γ-Fe, is also noticed when the reduction is performed at 1000 °C. It is proposed that the reduction of Fe^{3+}, which starts below 600 °C, proceeds in two steps, Fe^{3+} to Fe^{2+} (up to 900 °C) and Fe^{2+} to metallic Fe

(up to 1000 °C). The Fe^{2+} cations are believed to enter interstitial sites in the cubic zirconia lattice with a very short Fe^{2+}–Zr^{4+} distance, which would allow for a direct iron-zirconium metallic bond in the zirconia phase as reported by other researchers [33], Furthermore, we propose that as the reduction temperature is progressively increased and the reduction proceeds, there is also a phase partitioning, resulting in the formation of an Fe^{2+}-rich transient phase incorporating a small fraction of the Zr^{4+} ions, which is easily reduced into a metallic Fe/Zr phase accounting for the phase with a hyperfine field ∼200 kOe at RT (∼250 kOe at 80 K) which was detected by Mössbauer spectroscopy.

Acknowledgments

The authors would like to thank Mr. L. Datas for assistance in the FEG-SEM observations, which were performed at TEMSCAN, the "Service Commun de Microscopie Electronique à Transmission", Université Paul-Sabatier, Toulouse. F. L. G. thanks CONACYT (Mexico) for financial support. V. G. de R. thanks FWO––Flanders for financial support.

References

[1] R. Roy, Mat. Res. Symp. Proc. 286 (1993) 241.
[2] D. Chakravorty, Bull. Mater. Sci. 15 (1992) 411.
[3] S. Komarneni, J. Mater. Chem. 2 (1992) 1219.
[4] Ch. Laurent, A. Rousset, Key Eng. Mater. 108–110 (1995) 405.
[5] M. Nawa, T. Sekino, K. Niihara, J. Mat. Sci. 29 (1994) 3185.
[6] T. Ambrose, A. Gavrin, C.L. Chien, J. Magn. Magn. Mat. 116 (1992) L311.
[7] M. Pardavi-Horvath, L. Takacs, IEEE Trans. Magn. 28 (1992) 3186.
[8] P. Matteazzi, G. Le Caër, J. Am. Ceram. Soc. 75 (1992) 2749.
[9] R.A. Roy, R. Roy, Mater. Res. Bull. 19 (1984) 169.
[10] G.N. Subbanna, C.N.R. Rao, Mater. Res. Bull. 21 (1986) 1465.
[11] D. Chakravorty, Sadhana, 13 (1988)13.
[12] A. Chatterjee, D. Das, D. Chakravorty, K. Choudhury, Appl. Phys. Lett. 57 (1990) 1360.
[13] M. Verelst, K.R. Kannan, G.N. Subbanna, C.N.R. Rao, Ch. Laurent, A. Rousset, J. Mater. Res. 7 (1992) 3072.
[14] J. Petrullat, S. Ray, U. Schubert, G. Guldner, Ch. Egger, B. Breitscheidel, J. Non-Cryst. Solids 147-148 (1992) 594.
[15] X. Devaux, Ch. Laurent, A. Rousset, Nanostruct. Mater. 2 (1993) 339.
[16] Ch. Laurent, A. Rousset, M. Verelst, K.R. Kannan, A.R. Raju, C.N.R. Rao, J. Mater. Chem. 3 (1993) 513.
[17] Ch. Laurent, J.J. Demai, A. Rousset, K.R. Kannan, C.N.R. Rao, J. Mater. Res. 9 (1994) 229.
[18] A. Rousset, J. Sol. State Chem. 111 (1994) 164.
[19] Ch. Laurent, X. Devaux, A. Rousset, J. High Temp. Chem. Processes 3 (1994) 489.
[20] Ch. Laurent, Ch. Blaszczyk, M. Brieu, A. Rousset, Nanostruct. Mater. 6 (1995) 317.
[21] V. Carles, M. Brieu, A. Rousset, Nanostruct. Mater. 8 (1997) 529.
[22] V. Carles, Ch. Laurent, M. Brieu, A. Rousset, J. Mater. Chem. 9 (1999) 1003.
[23] O. Quénard, Ch. Laurent, M. Brieu, A. Rousset, Nanostruct. Mater. 7 (1996) 497.
[24] O. Quénard, E. De Grave, Ch. Laurent, A. Rousset, J. Mater. Chem. 7 (1997) 2457.
[25] P. Coquay, Ch. Laurent, A. Peigney, O. Quénard, E. De Grave, R.E. Vandenberghe, Hyp. Int. 130 (2000) 275.
[26] S.P. Jiang, S.H. Chan, J. Mater. Sci. 39 (2004) 405.
[27] F.R. Cichocki Jr., K.P. Trumble, Ceram. Trans. 74 (1996) 97.
[28] M. Wildan, H.J. Edrees, A. Hendry, Mater. Chem. Phys. 75 (2002) 276.
[29] S.C. Axtell, R. Schalek, J. Appl. Phys. 79 (1996) 5263.
[30] A. Ringuede, J.A. Labrincha, J.R. Frade, Sol. State Ionics 141-142 (2001) 549.
[31] F. Legorreta Garcia, V. Gonzaga de Resende, E. De Grave, A. Peigney, A. Barnabé, Ch. Laurent, Solid State Ionics, revised version submitted for publication.
[32] R.C. Garvie, P.S. Nicholson, J. Am. Ceram. Soc. 55 (1972) 303.
[33] P. Ghigna, G. Spinolo, U. Anselmi-Tamburini, F. Maglia, M. Dapiaggi, G. Spina, L. Cianchi, J. Am. Chem. Soc. 121 (1999) 301.
[34] S. Davison, R. Kershaw, K. Dwight, A. Wold, J. Sol. State Chem. 3 (1988) 47.
[35] V.R. Choudhary, S. Banerjee, S.G. Pataskar, Appl. Catal. A: Gen. 253 (2003) 65.